International Journal of Civil Engineering and Technology (IJCIET)
Volume 15, Issue 1, Jan-Feb 2024, pp. 47-65, Article ID: IJCIET_15_01_005
Available online at https://iaeme.com/Home/issue/IJCIET?Volume=15&Issue=1
ISSN Print: 0976-6308 and ISSN Online: 0976-6316
Impact Factor (2024): 21.69 (Based on Google Scholar citation)

STRUCTURAL HEALTH MONITORING FOR EXTERNAL RC NUCLEAR CONTAINMENT USING VARIOUS SETUP OF INNER ELECTRICAL RESISTIVITY MEASUREMENTS

Mostafa Hassan*
PhD Candidate at Ryerson University, 350 Victoria Street, Toronto-Ontario, Canada

Mohamed Ihab Sherif ELmasry
Professor of Structural Engineering, @AASTMT Abu-Qir Campus, Alexandria, Egypt

Nabil Hassan Elashkar
Professor of Structural Engineering, @AASTMT Abu-Qir Campus, Alexandria, Egypt
*Corresponding Author

ABSTRACT

Maintaining the integrity of nuclear power plant structures is critical for protecting the external environment. External reinforced concrete (RC) containment for the nuclear power plant is subjected to extreme airplane load. This research aims to monitor the cracks generated inside the wall of the external RC containment due to the impact of airplanes using embedded sensors located inside the core of the RC containment. This article simulates the reinforced concrete containment wall and the dome using ANSYS®. The wall is subjected to the impact of a Boeing 747-200C airplane at 30m height. The RC containment response was studied, and a proposed health monitoring technique was applied using embedded sensors to measure real-time electrical resistivity variations. An experimental study was conducted on different specimens that were made of heavyweight concrete. Cracks with different lengths were included inside the cracked specimens. The cracks are simulated inside laboratory specimens using failure criteria of concrete. The percentage change in inner electrical resistivity at different setups of measurements was deduced between the uncracked and different cracked specimens to measure the variations in electrical resistivity. Finally, the decimal logarithm resistivity anisotropy parameter at different measurement setups indicates the crack's presence and its direction inside the cracked specimens.

Keywords: Reinforced Concrete Containment, Airplane Impact, Health Monitoring, Inner Electrical Resistivity Measurements, Nuclear power plant, Airplane Impact.

Cite this Article: Mostafa Hassan, Mohamed Ihab Sherif ELmasry and Nabil Hassan Elashkar, Structural Health Monitoring for External RC Nuclear Containment Using Various Setup of Inner Electrical Resistivity Measurements, International Journal of Civil Engineering and Technology (IJCIET), 15(1), 2024, pp. 47-65.
https://iaeme.com/Home/issue/IJCIET?Volume=15&Issue=1

1. INTRODUCTION

Structural Health Monitoring (SHM) is defined as monitoring the integrity of structures and detecting damage in real-time. The applications of SHM can be assessed using different tools, such as dynamic response measurements, strain variations, and variations in electrical resistivity inside the concrete members. When applying structural health monitoring, continuous real-time data is collected for studying the damage propagation in structures. Moreover, electrical resistivity is considered a non-destructive testing method for Reinforced Concrete (RC) elements, and it can be used in detecting cracks [1, 2]. Electrical resistivity measurements were proposed earlier by Lataste et al. [3] for measuring the existing damage in concrete. Moreover, the advantages of the electrical resistivity technique are low cost, simplicity, and efficiency. The electrical resistivity of concrete is related to the microstructure of the cement matrix, its pore structure, porosity, and pore size distribution. In concrete, the current flows through the pores in the cement paste [4]. Aggregates are considered essentially inert. Generally, concrete is not a homogeneous conductor, and the flow of electric current will be heterogeneous. Heavyweight concrete is used in the shield for nuclear power plants and radiotherapy rooms [5]. The aggregate component of heavy-weight concrete contains a mixture of many heavy elements that play an important role in improving concrete shielding properties [5]. The conduction of electricity through concrete may take place in two ways, electronic and electrolytic. Thus, concrete electrical resistivity is a geometry-independent material property that describes the electrical resistance [6].

Several methods for measuring electrical resistivity were studied by Gowers and Millard, [6]. One of the most common methods used for measuring electrical resistivity is the Wenner probe method which is considered a reliable method [6, 7]. One of the factors that control electrical resistivity features in concrete is the hydration degree of the cement paste which would result in an increase in electrical resistivity over time. Moreover, the other influential factors affecting electrical resistivity measurements include the relative humidity, the concrete temperature, the ions concentration, and their mobility inside the pore solution [8]. Furthermore, when the interconnectivity of the pore network in concrete is broken, the movements of ions are disrupted. Accordingly, the presence of cracks in the concrete acts as a barrier between the movements of these ions, and thereby the electrical conductance of concrete [6]. The electrical resistivity of concrete can be measured using several means [9]. Moreover, the resistivity is often related to corrosion and the durability performance of concrete [10]. In general, the most common methods for measuring the electrical resistivity of concrete are as follows:

a. Two-Plate Electrode Method:

During testing, a low-frequency electrical current passes between the two electrodes through the entire specimen while the voltage drop is measured [8,11]. The electrical resistivity for the two-plate electrode method is conducted using equation (1).

$$\rho = \frac{R\,A}{L} \qquad (1)$$

b. Four-point electrode method (Wenner method):

The four-point electrode method is currently the most widely used technique for field concrete resistivity measurements. During testing, a low-frequency alternating current is applied between the two outer electrodes while the voltage drop is measured in the two inner electrodes [6]. The electrical resistivity for the Wenner method is calculated using equation (2).

$$\rho = 2\Pi \times a \times R \quad (2)$$

c. Four probes square configuration:

In this technique, the four probes are arranged in a square pattern on the outer surface of the concrete, and the electrical resistivity measurements can be calculated using equation (3) [4].

$$\rho = \frac{2\times\Pi\times a\times R}{2-\sqrt{2}} \quad (3)$$

d. Embedded electrode configuration

d.1. Linear Inner Electrical Resistivity Measurement (LIERM)

In this technique, the four probes are arranged on the same line pattern inside the concrete, as shown in Fig.1. Inner electrical resistivity can be calculated using equation (4) [12].

$$\rho = 4 \times \Pi \times a \times R \quad (4)$$

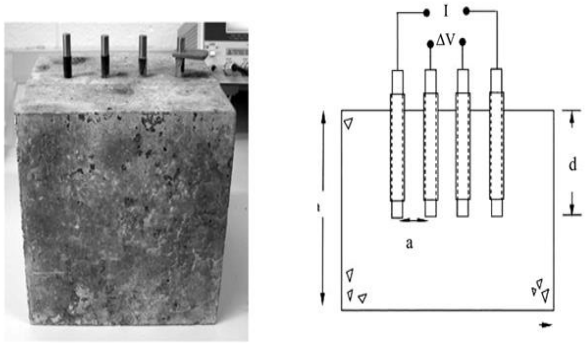

Fig.1. Linear inner electrical resistivity measurement for the concrete cube with embedded electrodes [12]

d.2.Square Inner Electrical Resistivity Measurement (SIERM)

In this technique, the four probes are arranged on a square pattern inside the concrete, as shown in Fig.2, and the SIERM is calculated using equation (5).

$$\rho = \frac{4\times\Pi\times a\times R}{2-\sqrt{2}} \quad (5)$$

where: ρ: electrical resistivity (Ohms.m), a: electrode spacing (m), and R: electrical current resistance (Ohm).

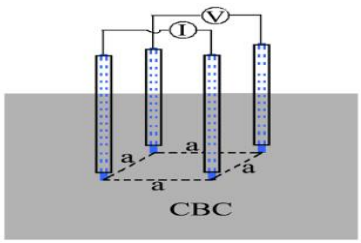

Fig. 2. Square inner electrical resistivity measurement configuration [2]

Specifically, two studied parameters are used based on electrical resistivity measurements in detecting damage as follows:

a- Percentage of change in electrical resistivity (% change in resistivity):

The Percentage change in electrical resistivity between any cracked specimen and the uncracked specimen in the same direction of measurement is calculated using equation (6) [1].

$$\%\ change\ in\ Resistivity = \frac{Rp-Rr}{Rr} \times 100 \qquad (6)$$

Where: R_p: resistivity for the cracked specimen, and R_r: resistivity for the uncracked specimen.

b- Decimal Logarithmic Resistivity Anisotropy (DLRA):

The Decimal Logarithmic Resistivity Anisotropy (DLRA) is calculated using equation (7) [1,2].

$$DLRA = \log_{10}\frac{R_v}{R_h} \quad \text{or} \quad DLRA = \log_{10}\frac{R_h}{R_v} \qquad (7)$$

Where: Rv: resistivity at the vertical current direction, R_h: resistivity at the horizontal current direction.

In practice, the change in electrical resistivity would indicate a crack. Thus, percentage change and DLRA are efficient parameters for detecting cracks [1, 2, 13, 14, 15].

This paper studies the response of the external RC containment subjected to the impact of the airplane Boeing 747-200c in terms of propagation of damage. This is the case where the cracks generated on the RC containment due to the airplane impact may lead to the escape of radiation into the external environment. The nonlinear response of the airplane impact is studied and then analyzed to identify the propagating damage in the containment structure from global and local behavior perspectives. The embedded sensors inside the core of the wall all over the containment are distributed in the vertical and circumference direction for detecting damage in real-time after the impact of the airplane Boeing 747-200c.

2. RESEARCH METHODOLOGY

2.1. Dimension of External RC Containment Used in ANSYS Model

A typical external RC nuclear containment consisting of a shell wall, dome, and base mat foundation is studied in this research. In this study, the thickness of the shell wall was considered 1.2m, and the inner side of the external containment was lined with a steel liner plate of a thickness of 9.375mm to prevent the escape of radioactive material into the external environment. The dome thickness was taken at 1.05m [16,17]. The dome is carried by the wall, and the load of the wall is transmitted into the fixed foundation [16,17]. The inner diameter of the containment was considered 45m, and the height of the cylindrical wall is nearly 36.5m from the top of the foundation level. The total height of the containment was considered 60m height. In this model, it is assumed that the connection between the foundation and the cylindrical wall is fixed as shown in Fig.3.

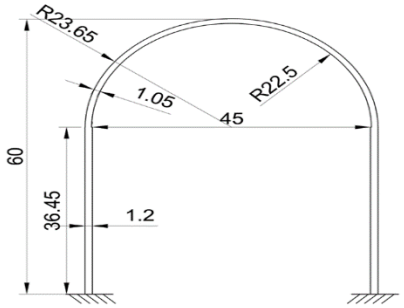

Fig. 3. Section elevation of the external RC containment

The containment is modeled using ANSYS®. The element used in ANSYS® to model RC members is Solid-65. Solid-65 element is used in 3D modeling of solids with or without reinforcing rebar. This solid element can indicate cracking in tension or crushing in compression. The element is defined by eight nodes having three degrees of freedom at each node: translations in the nodal x, y, and z directions. In addition, up to three different rebar specifications may be defined for Solid-65 elements. Moreover, the Solid-45 element is used in defining the inner steel liner plate. The element has plasticity, creep, swelling, stress stiffening, large deflection, and large strain capabilities.

In the recent model, the reinforcement was considered as membrane layers inside the wall and dome. For each layer, the steel type and the direction of reinforcement are specified. The reinforcement layers were considered continuous along the length of each layer. Reinforcement of the wall in the vertical direction is #18 spaced at 300mm, while in the circumference direction, the reinforcement is 2#18 spaced at 300 mm according to ACI Standard 359 in the year 2007. The element size in this model is nearly 2.0m×2.0m with a different thickness along the width of the wall with an acceptable aspect ratio. The total number of elements is 58830, and the total number of nodes is 62082.

2.2. Material Modeling of RC Containment

Concrete, steel reinforcement, and steel liner plates have different material models. The density of heavyweight concrete was taken as 3000 kg/m^3. The concrete was modeled as a multi-linear isotropic hardening plastic material, having its stress-strain curve as shown in Fig.4 [18]. The non-linear curve was obtained from equation (8) to equation (12).

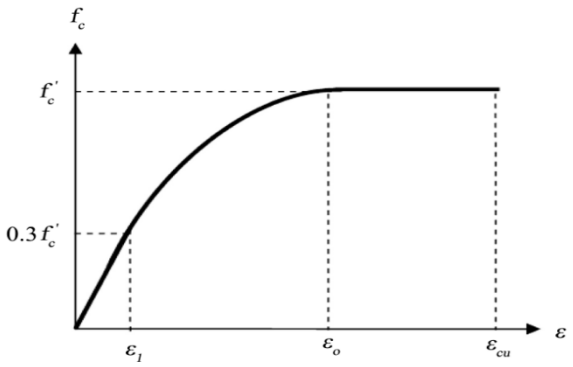

Fig. 4. Uniaxial compressive stress-strain curve for concrete in compression

$$f_c = E_c\,\varepsilon \qquad \text{for } 0 < \varepsilon < \varepsilon_1 \qquad (8)$$

$$f_c = f'_c \qquad \text{for } \varepsilon_0 < \varepsilon < \varepsilon_{cu} \qquad (9)$$

$$fc = \frac{E_c\,\varepsilon}{\left(1+\left(\frac{\varepsilon}{\varepsilon_0}\right)^2\right)} \qquad \text{for } \varepsilon_1 < \varepsilon < \varepsilon_0 \qquad (10)$$

$$\varepsilon_1 = (0.3\times f_c)/(E_c) \qquad (11)$$

$$\varepsilon_0 = (2f_c)/(E_c) \qquad (12)$$

The concrete is modeled in tension at which the rupture strength of concrete is illustrated as shown in Fig.5, and the cracked strain is calculated automatically from the modulus of elasticity of concrete. In addition, the concrete strength data are given as shown in Table 1. In the case of modeling the steel reinforcement bars and inner steel liner plate is assumed elastic and perfectly plastic. The elastic modulus for the steel reinforcement is 2×10^5 N/mm^2, and its Poisson ratio is 0.3.

In addition, the steel reinforcement is treated as a bilinear isotropic hardening plastic material with a yield stress of 400Mpa, whereas the yielding for the inner steel liner plate is 165Mpa [19]. The density of steel reinforcement and steel liner plate is considered 7785 kg/m^3.

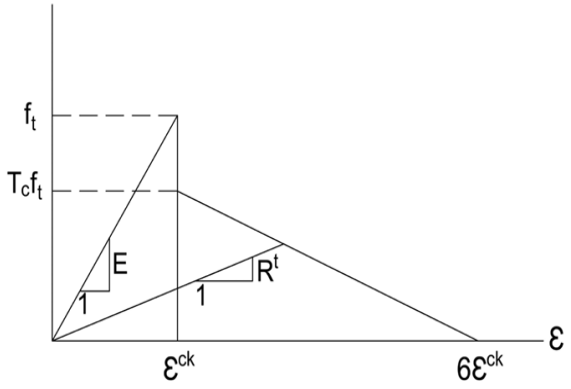

Fig. 5. Stress-strain curve for concrete in tension

Table 1. Concrete strength input data

Input strength parameters	Values
Open shear transfer coefficient	0.3
Closed shear transfer coefficient	0.9
Modulus of Elasticity of concrete (MPa)	36406.043
The Poisson ratio of concrete	0.2
Uniaxial cracking stress (Mpa)	4.8
Uniaxial crushing stress (Mpa)	60

2.2.1. Failure Criteria

The failure criterion for concrete due to a multi-axial stress state can be expressed as shown in equation (13) [20]. Moreover, if equation (13) is satisfied, the material will crack or crush. The failure surface is specified with a minimum of the two constants, ultimate uniaxial compressive and tensile strength [21].

$$\frac{F}{fc} - s \geq 0 \qquad (13)$$

Where:

F = function of the principal stress state (σ_{xp}, σ_{yp}, σ_{zp})

S = failure surface expressed in terms of principal stresses

f_c = uniaxial crushing strength

σ_{xp}, σ_{yp}, σ_{zp} = principal stresses in principal directions

2.3. Modelling the Impact of Boeing 747-200c Airplane

The Riera method [22] constructs a force time history to simulate an airplane crash impact. This is an approximate method for constructing a force time history for a projectile striking a rigid wall based on a known distribution of mass and crushing characteristics of the projectile along the length [23**,** 24].

The basic assumptions of the Riera method are as follows:

1) the target is rigid; 2) the axis of the missile is perpendicular to the target; 3) the missile is separated into two regions, one being uncrushed and moving with velocity (v) and the other region being crushed with zero velocity; 4) all crushing takes place within a local region adjacent to the rigid target; 5) the crushing or material behavior of the missile is rigid perfectly plastic.

The most dangerous impact is that of the airplane with maximum mass during impact. It is assumed that the crushing force is calculated using equation (14). Crushing force (R_e) depends on the local crushing strength of the fuselage [24].

$$Re=A\ \sigma_y \quad (14)$$

where: A is the effective area of the crushing section and σ_Y is the yielding stress of the material.

The crushing force Re(x) induces instantaneous and homogenous deceleration (dv/dt) in the remaining uncrushed part. If the total mass of the airplane is (M) and the mass of the crushed part is m(x), then, the deceleration and crushing force are given as shown in equation (15). It is assumed that there is no rebound of the crushed part [25].

$$[M - m(x)]\ \frac{dv}{dt} = -Re(x) \quad (15)$$

The force that is acting on the target is conducted by Riera's formula as shown in equation (16) [25].

$$F=Re(x)+\mu(x)\ v^2 \quad (16)$$

Where: the aircraft is modeled by a stick with mass distribution $\mu(x)$ and crushing force Re(x), where x is the distance along the fuselage from the airplane nose up to the current section that undergoes the crushing.

The impact of the Boeing 747-200c was considered in this research concentrated at 16 nodal points at an average distance of 30m above the foundation level of the external RC containment. The impact area of the Boeing 747-200C airplane is assumed to be $36m^2$ according to the maximum fuselage diameter of the airplane which is 6.5 m. In addition, the velocity of the Boeing 747-200c airplane is 968 km/hr. The represented load-time curve for Boeing 747-200c is shown in Fig.6 [24].

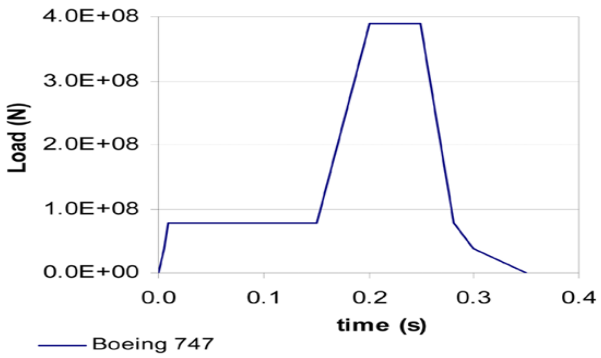

Fig.6. Load time curve for Boeing 747-200c at 269 m/sec [24]

3. ANALYSIS OF RESULTS

3.1. Response of RC Containment

The maximum displacement occurs at the point of impact of the airplane which reaches a value of 46.658 mm at a time of 0.2 seconds, due to the impact of the airplane Boeing 747-200c at a speed of 269 m/sec as shown in Fig.7.

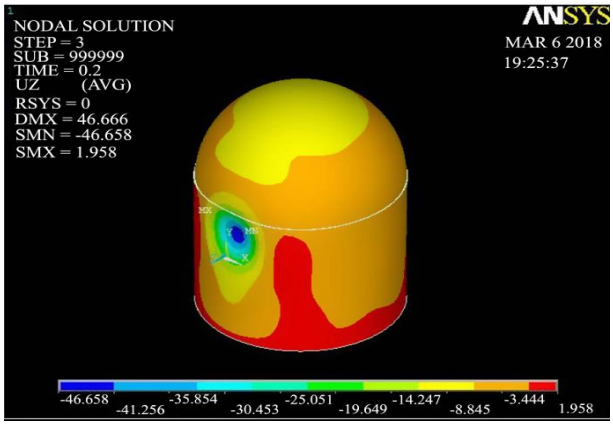

Fig.7. The maximum displacement of RC containment in the direction of loading at the time of 0.2 second

The displacement of RC containment in the direction of loading is maximum at the impact region and vanishes at an approximate distance of 18 m along the outer circumference direction from the right and left-hand side of the impact region as shown in Fig.8.

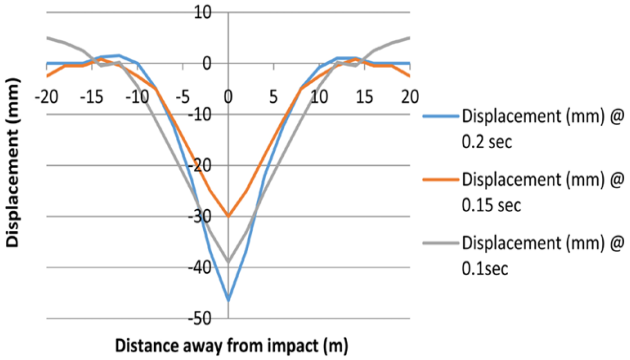

Fig. 8. Displacement of RC containment in the direction of loading due to the impact of Boeing 747-200C at a different time of impact

The types of cracks at the containment are shear cracks that appear away from the impact region and flexure cracks that appear at the fixation of the RC foundation with the wall as shown in Fig.9. The region of the impact of an airplane on the external RC containment has a local failure in the concrete element which makes spalling of concrete at this region of containment. The rest of the RC containment has been fully intact.

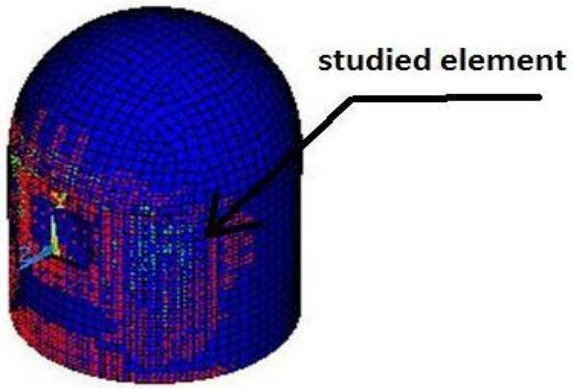

Fig. 9. The shape of cracks on RC containment due to the impact of the Boeing 747-200C airplane

3.2. Laboratory Experimental Simulation

Laboratory RC specimens were prepared by taking a part of two elements from the ANSYS model as shown in Fig. 10 (a). Failure criteria of concrete were applied on common edge nodes between two elements as shown in Fig. 10 (b) to trace the crack propagation length concerning the corresponding time of airplane impact. The element size in the Ansys is 2.068m ×2.025m with different thicknesses having an acceptable aspect ratio as shown in Fig.10 (b). Apart from large two elements were taken to be suitable for casting it in a laboratory of dimension (0.69m ×0.66 m ×1.21 m) as shown in Fig.10 (a). The application of the square inner electrical resistivity on three different cracked specimens, represented at different times of (0.1, 0.11, 0.14) seconds of airplane impact, while the uncracked specimen is at time zero of airplane impact.

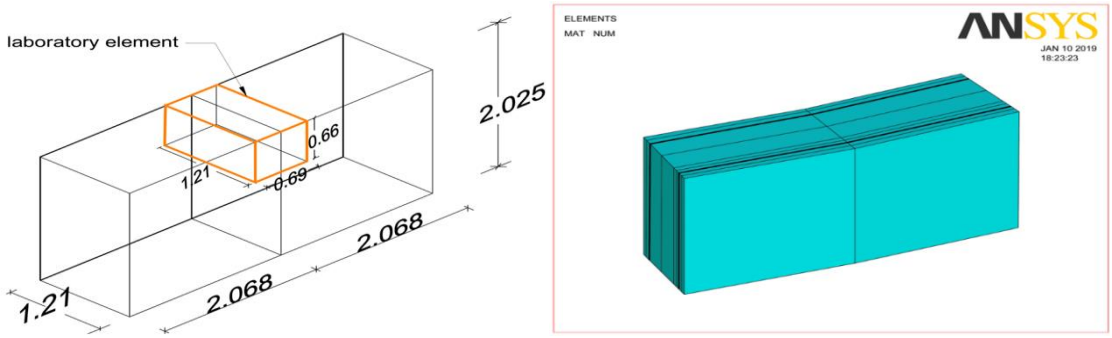

(a) Laboratory element (b) ANSYS elements

Fig.10. Laboratory elements versus ANSYS element

An element has been chosen at the tension region away from the impact of the Boeing 747-200C airplane, this region comes out and acts as a rigid support, the chosen element carries vertical and horizontal cracks as shown in Fig.11.

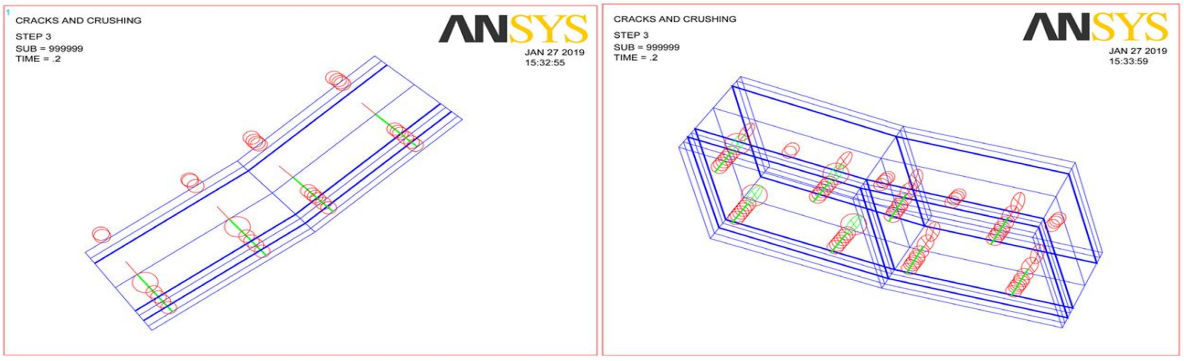

(a) Plan of cracked element (b) 3D cracked element

Fig.11. Cracked elements for RC containment that it is located away from the impact region of the airplane

The length of the vertical crack was concluded from the domains of failure criteria of concrete applied on common nodes between two elements chosen for concrete to predict the average length of vertical crack at a different time of airplane impact as shown in Fig.12.

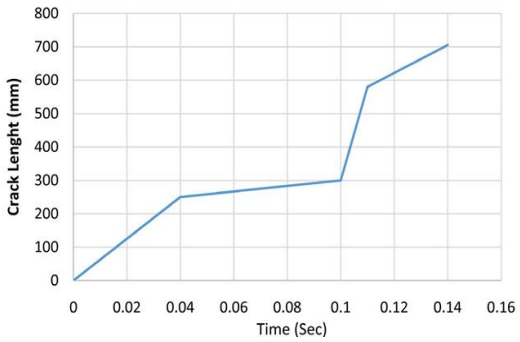

Fig.12. Vertical crack length versus the time of the airplane impact

Each laboratory RC specimen carries eight red copper bulbs of dimension (1cm×1.5cm×1cm). Sensors are drilled in 3 directions to fix it with the formwork in the laboratory in various directions. The spacing between the sensors in configuration is 300mm, inside each laboratory specimen. Laboratory specimens include in its core two vertical square setup configurations spaced at 300 mm as shown in Fig.13 according to Gowers and Millard, [6]. The copper sensors are connected with the electric wires, the diameter of the electric wire is 1.5 mm, and at each end of the wire, 5cm of the plastic cover was removed. One end of the wire is at the sensor and the other end is outside the concrete specimen to measure electrical resistivity. The square inner electrical resistivity measurement was applied to the uncracked and cracked specimens.

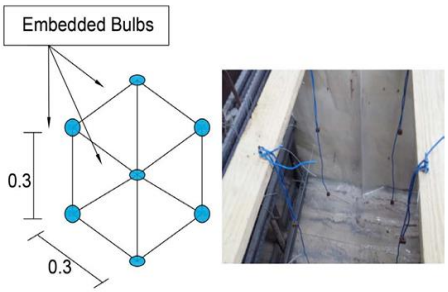

Fig.13. Sensor's configuration inside the laboratory specimens

Apart from the two elements in ANSYS were simulated in the laboratory to replicate the real-time for the crack propagation. The dimensions for the laboratory RC specimens are (0.69 m× 0.66 m ×1.21 m) consisting of embedded sensors located in two configurations at the core of the RC wall. The distance between the outer and the inner setup configuration is 300 mm as shown in Fig.14.

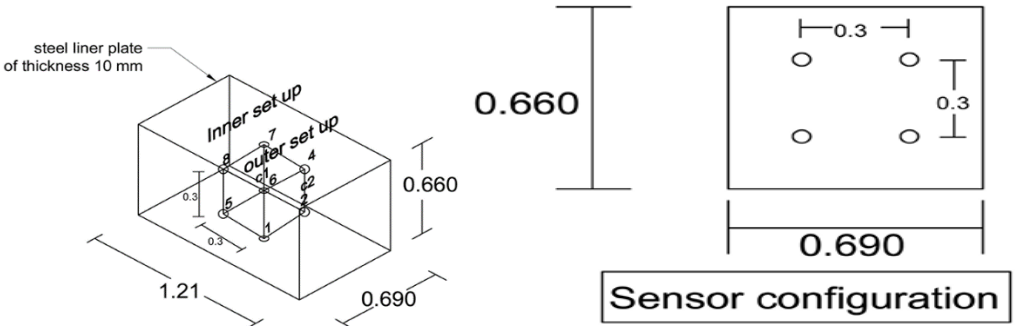

(a) Three-dimensional for the RC specimen specimen

(b) Section elevation for the core of the

Fig.14. Laboratory specimen with embedded sensors

The laboratory RC specimens consist of vertical and horizontal steel reinforcement on each side of the specimen and the inner steel liner plate is embedded at the back of the specimens as shown in Fig.15.

Fig.15. Steel reinforcement for the laboratory RC specimen

The chosen two elements from ANSYS are cracked in vertical and horizontal directions locally. The three cracked specimens carry only vertical cracks in this research. In the first specimen, the vertical crack is away from the front sensors by 150mm at a time 0.1 second of impact load as shown in Fig.16 (a). In the second specimen, the vertical crack cuts the first square sensor configuration by 130 mm at a time of 0.11 seconds as shown in Fig.16 (b). Moreover, In the third specimen, the vertical crack cuts the first square configuration by 255 mm at a time of 0.14 seconds as shown in Fig.16 (c). The vertical crack length increases over time as the impact load increases as shown in Fig.16.

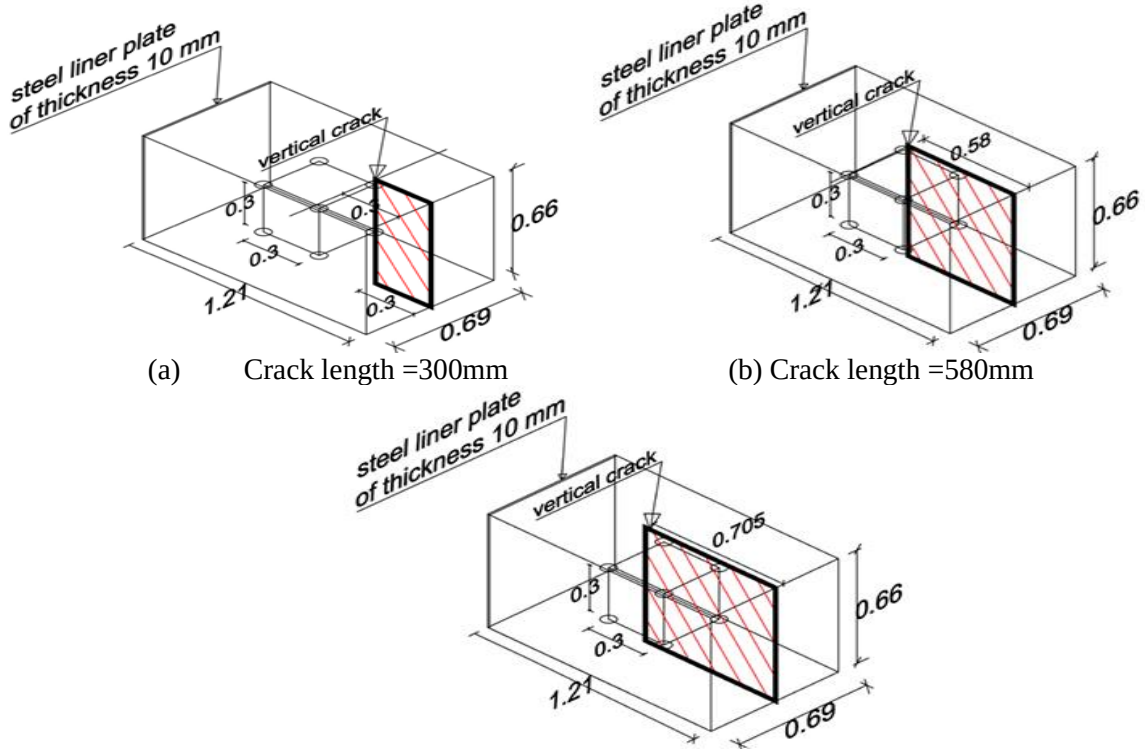

(a) Crack length =300mm (b) Crack length =580mm

(c) Crack length =705mm

Fig.16. Lengths of vertical cracks inside the laboratory RC specimen at different times of impact load

The concrete mix design has a constant water-to-cement ratio of 0.35 and a superplasticizer was used to maintain a constant slump. The concrete mix consists of ordinary Portland cement content equal to 450 kg/m^3 and the sand-to-total aggregate ratio is 40% adjusted for the concrete mixture. The nominal maximum size of coarse aggregates is 40mm. Experimental results revealed that the concrete mix containing hematite coarse aggregate along with 10 % silica fume reaches the highest compressive strength values exceedingly over 60 Mpa according to Ouda, [26].

3.3. Detecting Cracks Using Square Inner Electrical Resistivity at Different Configurations for Sensors

The measurements of the inner electrical resistivity were taken once perpendicular to the crack plane in the horizontal direction, and the other one parallel to the crack plane in the vertical direction according to the outer and inner square setup configuration over the time of impact. In addition, the resistivity measurements were measured in a diagonal setup configuration between the outer and inner sensors setup and in the radial direction of the RC wall which is parallel to the crack plane. The target of this research is to apply the square inner electrical resistivity measurement technique as a nondestructive testing method inside the core of the RC wall to detect the presence of cracks. Two parameters detected the damage, especially the cracks. The first parameter used is the percentage change in electrical resistivity between different cracked specimens and the uncracked specimen. The second parameter used is Decimal logarithm Resistivity Anisotropy (DLRA) which gives a good indication of the presence and the direction of the crack inside the RC wall.

It was concluded that the percentage change in electrical resistivity between the cracked specimen of 705mm crack length and the uncracked specimen in the outer square setup reached a value of 413.33% as shown in Fig.17(a), (b) at which the direction of current is perpendicular to the crack plane.

In the inner setup configuration, the percentage change of electrical resistivity between the cracked specimen of crack length 705mm and the uncracked specimen reached a value of 30% as shown in Fig.17 (c), (d) at which the crack is away from sensors.

The percentage change in electrical resistivity between the cracked specimen of 705mm crack length and the uncracked specimen in the outer vertical square setup reached a value of -76.67% as shown in Fig.17(e), (f); where the direction of current is parallel to the crack plane. Moreover, the percentage change in electrical resistivity between the cracked specimen of 705mm crack length and the uncracked specimen in the inner vertical setup reached a value of -40 % as shown in Fig.17 (g), (h), where the crack is away from sensors. In addition, the percentage change in electrical resistivity between the cracked specimen of a crack length of 705 mm and the uncracked specimen in the radial direction of the wall which is parallel to the crack plane reached a value of -77.58% as shown in Fig.17 (i), (j), (k), (l). Thus, the percentage change in electrical resistivity is decreased in the direction parallel to the crack plane according to Lataste et al. [3]. The percentage change in electrical resistivity between the cracked specimen of 705mm crack length and the uncracked specimen in the outer horizontal setup configuration reached a value of 320% as shown in Fig. 17 (m), (n) at which the crack is perpendicular to the direction of the current. Finally, the percentage of change in electrical resistivity between the cracked specimen and the uncracked specimen in diagonal setup configuration reached a value of 210% as shown in Figure 17 (o), (p), (q), (r) at which the direction of current cuts the crack.

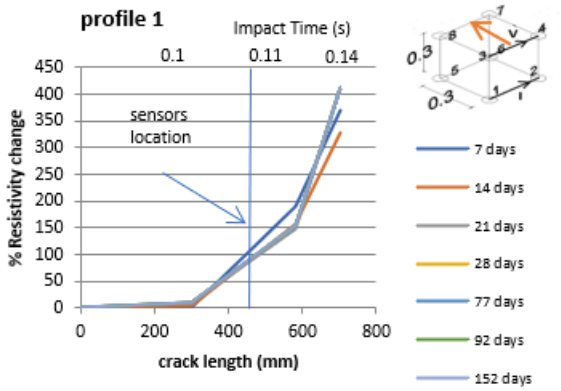
profile 1
Impact Time (s)
0.1
0.11
0.14
sensors location
% Resistivity change
crack length (mm)
7 days
14 days
21 days
28 days
77 days
92 days
152 days

(a)

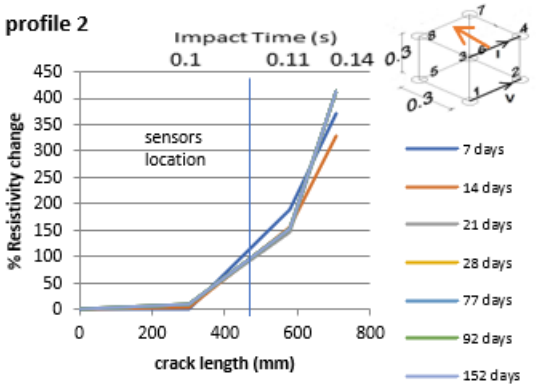
profile 2
Impact Time (s)
0.1
0.11
0.14
sensors location
% Resistivity change
crack length (mm)
7 days
14 days
21 days
28 days
77 days
92 days
152 days

(b)

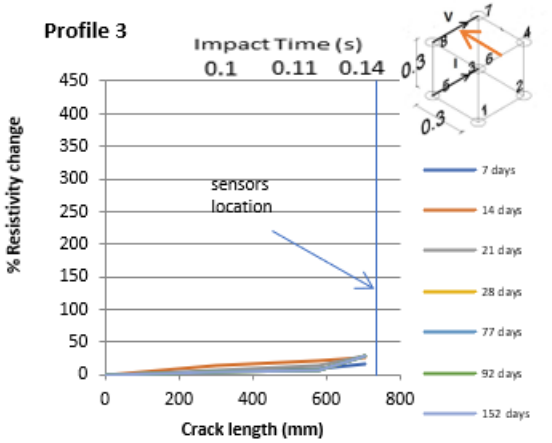
Profile 3
Impact Time (s)
0.1
0.11
0.14
sensors location
% Resistivity change
Crack length (mm)
7 days
14 days
21 days
28 days
77 days
92 days
152 days

(c)

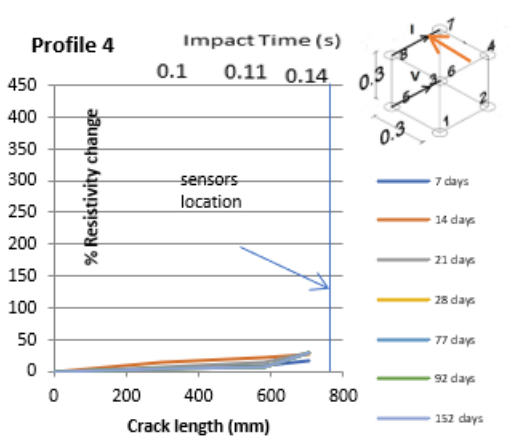
Profile 4
Impact Time (s)
0.1
0.11
0.14
sensors location
% Resistivity change
Crack length (mm)
7 days
14 days
21 days
28 days
77 days
92 days
152 days

(d)

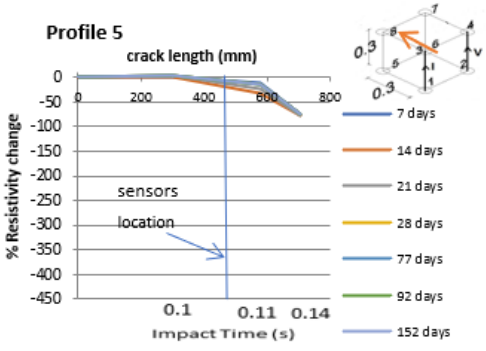
Profile 5
crack length (mm)
sensors location
% Resistivity change
Impact Time (s)
0.1
0.11
0.14
7 days
14 days
21 days
28 days
77 days
92 days
152 days

(e)

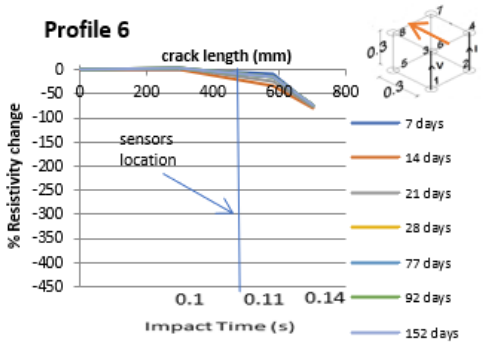
Profile 6
crack length (mm)
sensors location
% Resistivity change
Impact Time (s)
0.1
0.11
0.14
7 days
14 days
21 days
28 days
77 days
92 days
152 days

(f)

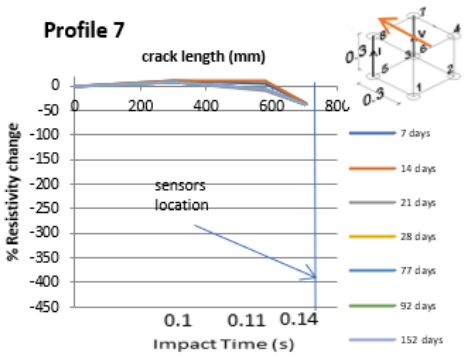
Profile 7
crack length (mm)
sensors location
% Resistivity change
Impact Time (s)
0.1
0.11
0.14
7 days
14 days
21 days
28 days
77 days
92 days
152 days

(g)

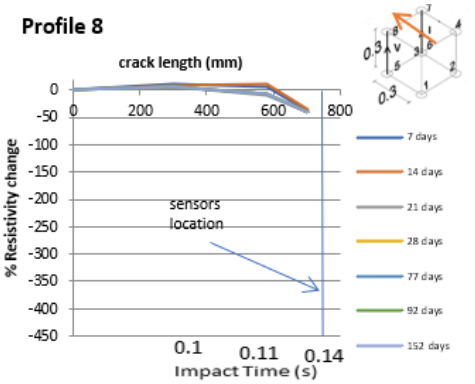
Profile 8
crack length (mm)
sensors location
% Resistivity change
Impact Time (s)
0.1
0.11
0.14
7 days
14 days
21 days
28 days
77 days
92 days
152 days

(h)

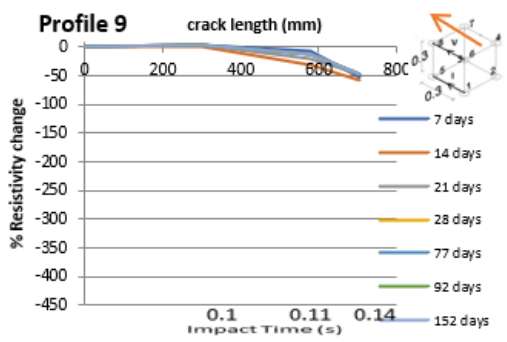
Profile 9
crack length (mm)
% Resistivity change
Impact Time (s)
7 days
14 days
21 days
28 days
77 days
92 days
152 days

(i)

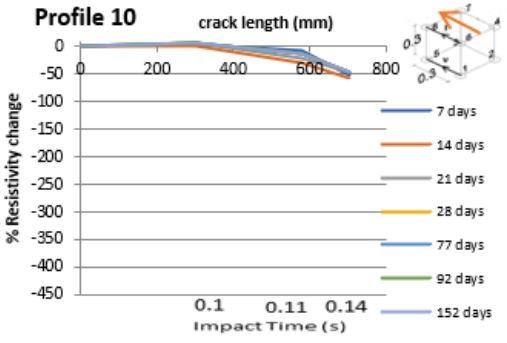
Profile 10
crack length (mm)
% Resistivity change
Impact Time (s)
7 days
14 days
21 days
28 days
77 days
92 days
152 days

(j)

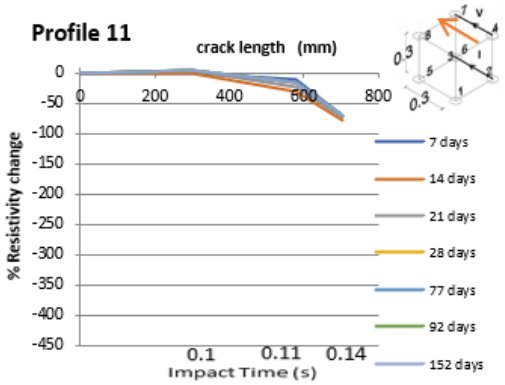
Profile 11
crack length (mm)
% Resistivity change
Impact Time (s)
7 days
14 days
21 days
28 days
77 days
92 days
152 days

(k)

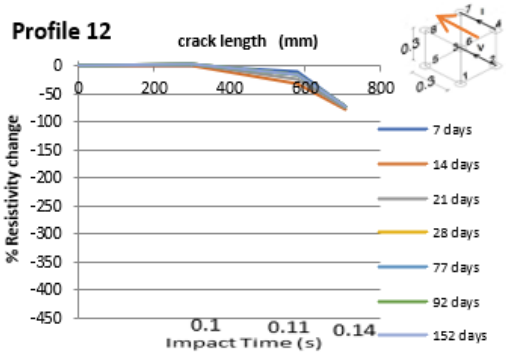
Profile 12
crack length (mm)
% Resistivity change
Impact Time (s)
7 days
14 days
21 days
28 days
77 days
92 days
152 days

(l)

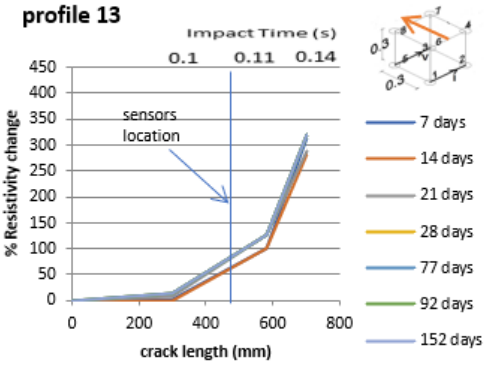
profile 13
Impact Time (s)
sensors location
% Resistivity change
crack length (mm)
7 days
14 days
21 days
28 days
77 days
92 days
152 days

(m)

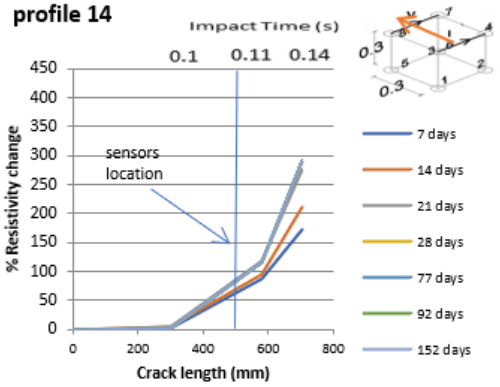
profile 14
Impact Time (s)
sensors location
% Resistivity change
Crack length (mm)
7 days
14 days
21 days
28 days
77 days
92 days
152 days

(n)

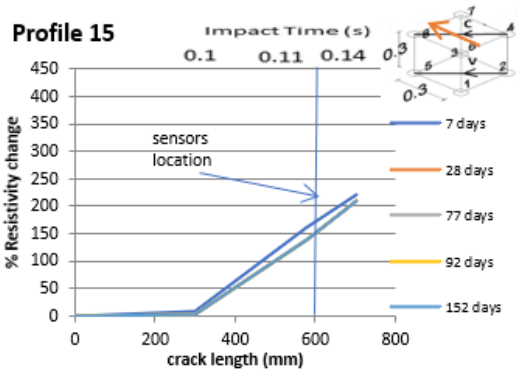
Profile 15
Impact Time (s)
sensors location
% Resistivity change
crack length (mm)
7 days
28 days
77 days
92 days
152 days

(o)

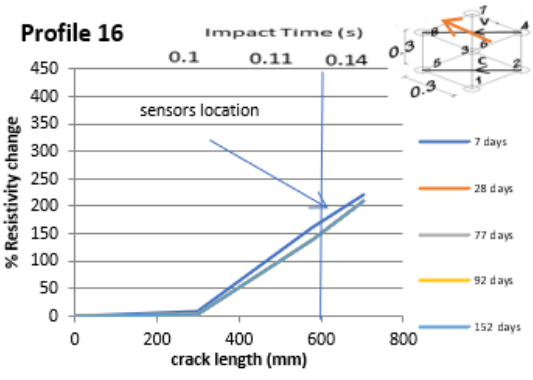
Profile 16
Impact Time (s)
sensors location
% Resistivity change
crack length (mm)
7 days
28 days
77 days
92 days
152 days

(p)

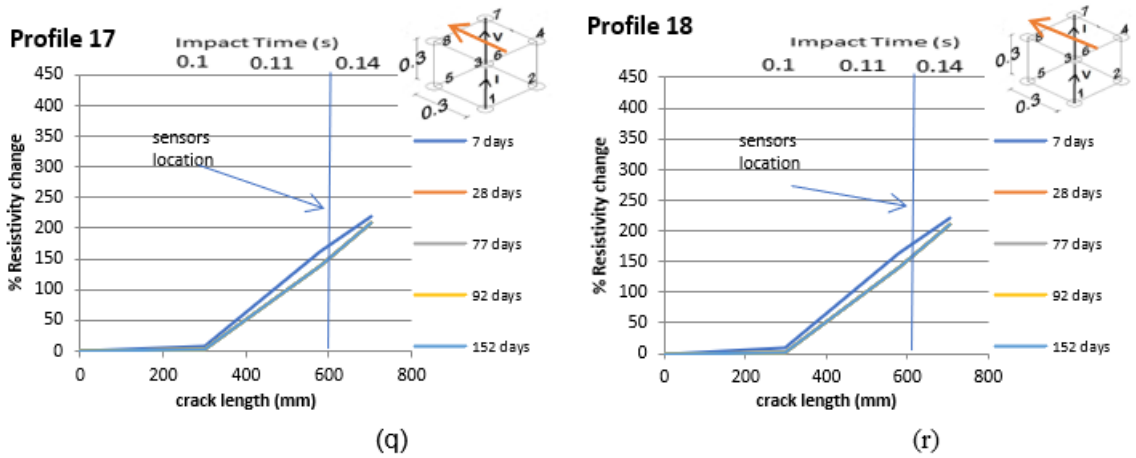

Fig. 17. Different crack lengths at various times of impact versus the percentage change in electrical resistivity at different setup configurations

3.4. Detecting the Crack Length Using the Decimal Logarithm Resistivity Anisotropy (DLRA) at Different Configurations of Sensors

The second parameter used to detect the crack is the Decimal Logarithm Resistivity Anisotropy (DLRA) for concrete by dividing resistivity in the direction perpendicular to the crack plane to the other measurement parallel to the crack plane. DLRA detected the presence and direction of the crack inside the RC specimen. It was concluded that the maximum DLRA reached a value of 1.3 when dividing resistivity in the direction perpendicular to the crack plane to resistivity which is parallel to the crack plane in the outer setup as shown in Fig.18(a).

The DLRA in the inner square setup at which the crack doesn't reach the inner setup configuration its value is too small compared to the outer square setup as shown in Fig.18(b) and reached a value of 0.335. Moreover, DLRA measurements between either lower or upper horizontal resistivity which are perpendicular to the crack plane to radial resistivity on either the left or right-hand side which is parallel to the crack reached a maximum value of 1.3 and it indicates the presence of the crack as shown in Fig.18(c),(d),(e),(f). The measurement of DLRA between inner horizontal resistivity to radial resistivity (parallel to the crack plane) on either the left- or right-hand side gives a small value of DLRA reaching a value of 0.389 as shown in Fig.18 (g), (h). Furthermore, the measurement of DLRA between outer vertical resistivity which is parallel to the crack plane to radial resistivity either on the left or right-hand side which is parallel to the crack plane gives a minimum indication of the presence of a crack as shown in Fig.18 (i),(j),(k),(l) because the resistivity is the same in both directions which is parallel to the crack plane.

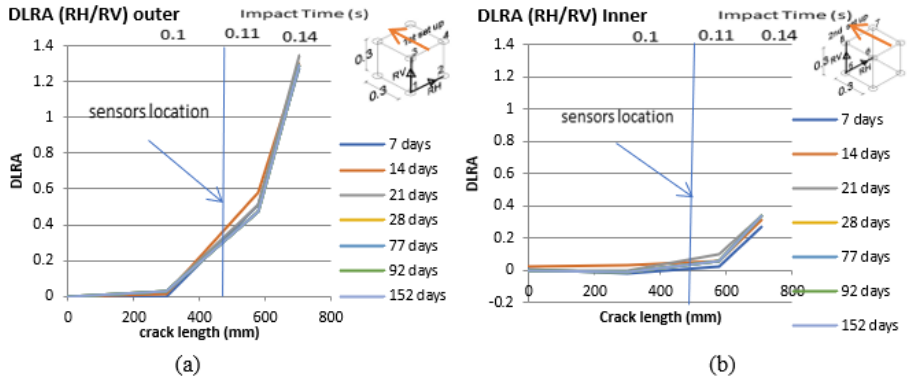

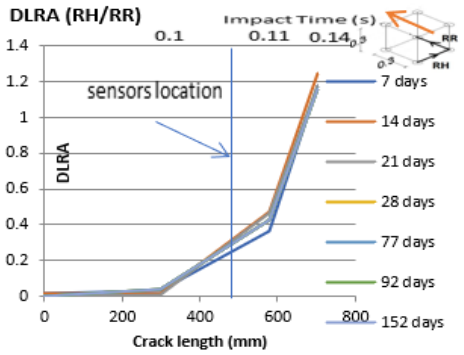
DLRA (RH/RR)
Impact Time (s)
0.1
0.11
0.14
sensors location
DLRA
Crack length (mm)
7 days
14 days
21 days
28 days
77 days
92 days
152 days

(c)

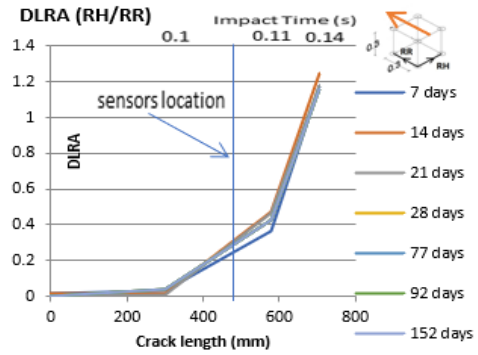
DLRA (RH/RR)
Impact Time (s)
0.1
0.11
0.14
sensors location
DLRA
Crack length (mm)
7 days
14 days
21 days
28 days
77 days
92 days
152 days

(d)

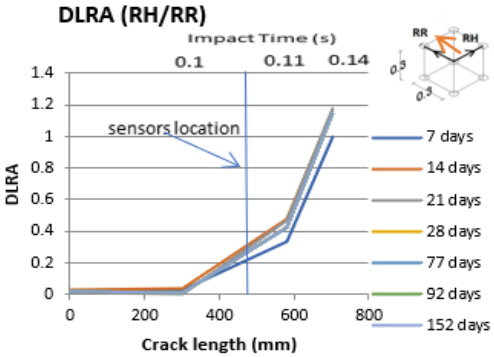
DLRA (RH/RR)
Impact Time (s)
0.1
0.11
0.14
sensors location
DLRA
Crack length (mm)
7 days
14 days
21 days
28 days
77 days
92 days
152 days

(e)

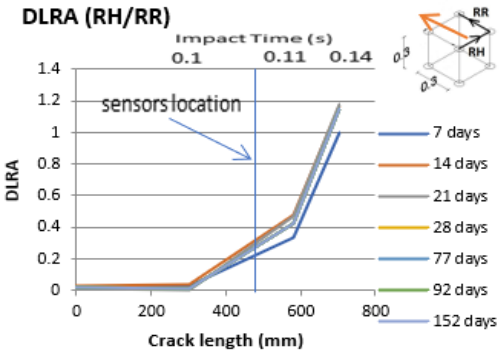
DLRA (RH/RR)
Impact Time (s)
0.1
0.11
0.14
sensors location
DLRA
Crack length (mm)
7 days
14 days
21 days
28 days
77 days
92 days
152 days

(f)

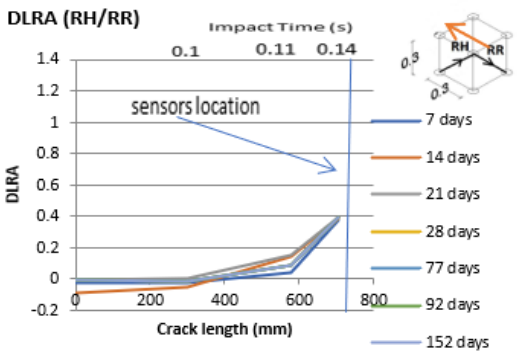
DLRA (RH/RR)
Impact Time (s)
0.1
0.11
0.14
sensors location
DLRA
Crack length (mm)
7 days
14 days
21 days
28 days
77 days
92 days
152 days

(g)

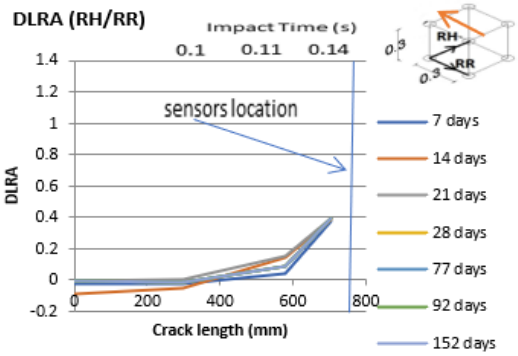
DLRA (RH/RR)
Impact Time (s)
0.1
0.11
0.14
sensors location
DLRA
Crack length (mm)
7 days
14 days
21 days
28 days
77 days
92 days
152 days

(h)

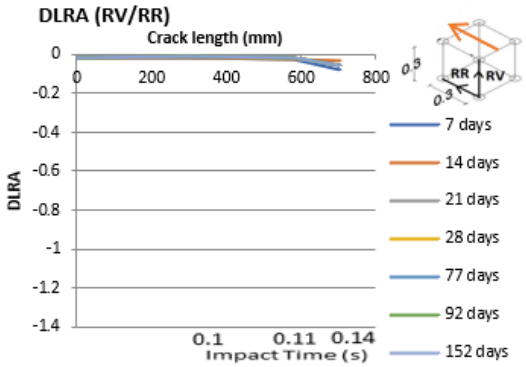
DLRA (RV/RR)
Crack length (mm)
DLRA
Impact Time (s)
0.1
0.11
0.14
7 days
14 days
21 days
28 days
77 days
92 days
152 days

(i)

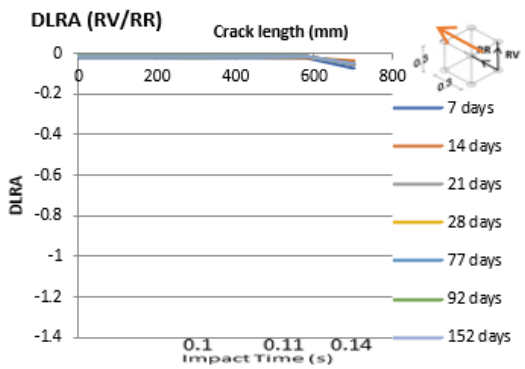
DLRA (RV/RR)
Crack length (mm)
DLRA
Impact Time (s)
0.1
0.11
0.14
7 days
14 days
21 days
28 days
77 days
92 days
152 days

(j)

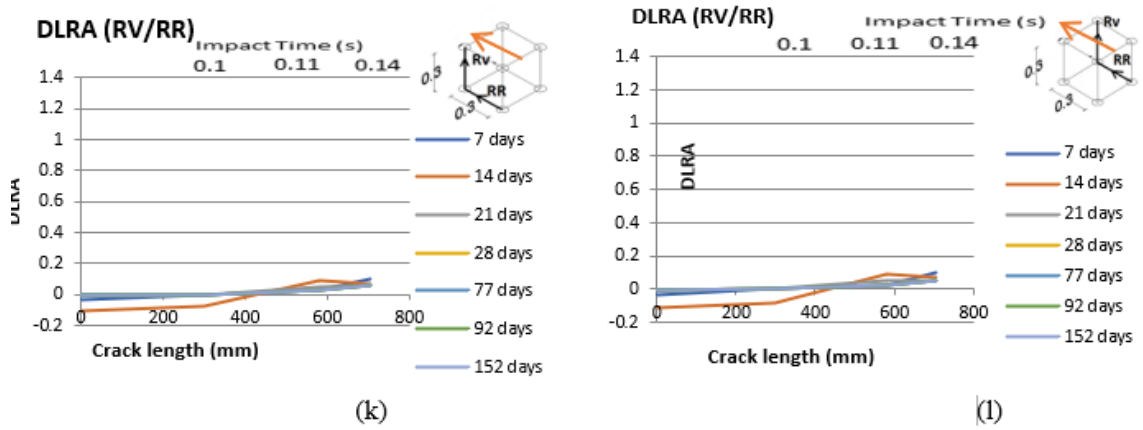

Fig.18. DLRA versus various crack lengths that correspond to the time of airplane impact at different setup configurations.

4. CONCLUSIONS

External RC containment became globally stable after the impact of the airplane Boeing 747-200C, and some elements were fully damaged in the impact region only. Square inner electrical resistivity measurement is used as a structural health monitoring technique to detect the cracks inside the core of the concrete wall by using red copper sensors. Moreover, the copper sensors are distributed along the intermediate circumference of the wall and along the vertical direction of the wall spaced 300mm vertically and radially center to center between each sensor.

The crack propagation inside the studied element was deduced using the failure criteria of concrete which is built in ANSYS according to the domains of failure criteria. The two parameters that are used to detect the presence of cracks inside concrete walls are the percentage of change in electrical resistivity between the cracked specimens and the uncracked specimen, the second parameter is Decimal Logarithm Resistivity Anisotropy (DLRA).

- It was observed that when the current cuts the crack plane which is perpendicular to the crack plane, the percentage change in electrical resistivity reached a maximum value of 413.33%, while when the current moves in the direction parallel to the crack plane, the percentage change in electrical resistivity is decreased, and reached a value of -77.58%.
- The percentage change in electrical resistivity in diagonal setup configuration reached a value of 210% between the cracked specimen of 705mm crack length and the uncracked specimen. Furthermore, when the electrical current moves perpendicular to the crack plane, it gives a good indication of the presence of a crack.
- DLRA measurements give a maximum value and reach a value of 1.3 when dividing the resistivity in the direction perpendicular to the crack plane by resistivity which is parallel to the crack plane. Finally, DLRA detects the presence of a crack inside the wall and gives the directions of the crack plane from its measurements. The proposed technique of sensors inside the RC external wall of the nuclear power plants successfully detects the variation in electrical resistivity between the cracked and uncracked parts of external RC containment over time of the impact continuously.

Acknowledgments

I would like to thank our professors Mohamed Ihab Elmasry and Nabil Hassan El Ashkar for their Support and guidance in this research, and I would like also to thank the Arab Academy for Science, Technology and Maritime Transport for doing this experimental work in the heavyweight structural laboratory which is related to Construction and Building Engineering Department at Abu-Qir Campus.

Conflicts of Interest

The authors declare no conflicts of interest regarding the publication of this paper.

REFERENCES

[1] Elmasry, M.I.S., ElAshkar, N.H., Alasadi, M.F.A. (2012). Damage Identification in RC Beams Using Internal Electrical Resistivity Measurements, ICSDEC 2012: Developing the Frontier of Sustainable Design, Engineering, and Construction, pp.801-809. https://doi.org/10.1061/9780784412688.096.

[2] Elashkar, N.H., Elmasry, M.I.S., Anndif, M.A.A. (2012). Damage Detection and Localization by Interpretation of Square Inner Electrical Resistivity Measurements. Sixth European Workshop on Structural Health Monitoring.

[3] Lataste, J.F., Sirieix, C., Breysse, D., and Frappa, M. (2003). Electrical resistivity measurement applied to cracking assessment on reinforced concrete structures in civil engineering, NDT & E International, vol. 36, 383-394.

[4] Madhavi, T.C., and Annamalai, S. (2016). Electrical Conductivity of Concrete. ARPN Journal of Engineering and Applied Sciences, 11 (9), pp.5979-5982.

[5] Mehta, K.P., and Monteiro, P.J. (2006). Concrete Microstructure, Properties, and Materials, Electronic Book, pp.529-531.

[6] Gowers, K.R., and Millard, S.G. (1999). Measurement of Concrete Resistivity for Assessment of Corrosion Severity of Steel Using Wenner Technique, ACI Material Journal, 96, pp.536-541. https://doi.org/10.14359/655.

[7] Sengul, O., and Gjorv, O.E. (2009). Effect of Embedded Steel on Electrical Resistivity Measurements on Concrete Structures, ACI Materials Journal, 106, pp.11-18.

[8] Shahroodi, A. (2010). Development of Test Methods for Assessment of Concrete Durability for Use in Performance-Based Specifications. Master of Applied Science, University of Toronto, Canada.

[9] Polder, R.B. (2000). Electrochemical techniques for measuring metallic corrosion. RILEM TC 154-EMC, Materials, and Structures, 33, pp.603-611.

[10] Ferreira, R.M., Jalali, S. (2010). NDT Measurements for the Prediction of 28-day Compressive Strength. NDT & E International, 43, pp.55-61.

[11] Morris, W., Moreno, E.I., and Sagues, A.A. (1996). Practical Evaluation of Resistivity of Concrete in Test Cylinders Using a Wenner Array Probe, Cement and Concrete Research, 26, pp.1779-1787.

[12] McCarter, W.J., Starrs, G., Kandasami, S., Jones, R., and Chrisp, M. (2009). Electrode Configuration for Resistivity Measurements on Concrete, ACI Materials Journal, 106, pp.258-264. https://doi.org/10.14359/56550.

[13] Hassaan, M., Elmasry, M.I.S, El Ashkar, N. (2021). Structural Health Monitoring for Reinforced Concrete Containment Using Inner Electrical Resistivity Method, Open Journal of Civil Engineering, 11 (3), pp.317-341. https://doi.org/10.4236/ojce.2021.113019.

[14] Hassaan, M., Elmasry, M.I., Ashkar, N.E. (2021). Effect of Impact Boeing 707-320 on External RC Containment of Nuclear Power Plant for Different Compressive Strength of Concrete, Saudi Journal of Civil Engineering, 5(8), pp.282-304. https://doi.org/10.36348/sjce.2021.v05i08.004.

[15] Hassaan, M., Elmasry, M.I., Ashkar, N.E. (2021). Detection of Cracks in Heavy Weight Concrete Using Inner Electrical Resistivity Method, Saudi Journal of Civil Engineering, 5(9), pp.355-366. https://doi.org/10.36348/sjce.2021.v05i09.004.

[16] Elmasry, M.I.S., Alashkar, N.H., Hassan, M.M. (2019). Stability of Concrete Containments of Nuclear Plants Under Jet Impact Loads. In: Rodrigues, H., Elnashai, A. (eds) Advances and Challenges in Structural Engineering. GeoMEast 2018. Sustainable Civil Infrastructures. Springer, Cham. https://doi.org/10.1007/978-3-030-01932-7_30.

[17] CZERNIEWSKI, S. (2009). The Feasibility of Modern Technologies for Reinforced Concrete Containment Structures of Nuclear Power Plants, a Report of master science, Kansas State University.

[18] Salman, W.D. (2015). Nonlinear Behavior of Reinforced Concrete Continuous Deep Beam, International Journal of Engineering Research & Technology (IJERT), 4, ISSN: 2278-2281.

[19] Teh Hu, H., XuLin, j. (2015). Ultimate analysis of PWR prestressed concrete containment under long-term prestressing loss. Annals of Nuclear Energy, 87, pp.500-510.

[20] William, K.J. and Warnke, E.P. (1974). A constitutive model for the tri-axial behavior of concrete. IABSE reports the working commissions. BERGAMO, ITALY.

[21] ANSYS12 (2012). Theory Reference Manual

[22] Riera, J.D. (1968). On the stress analysis of structures subjected to aircraft impact forces. Nuclear Engineering Design, 8, pp.415–426.

[23] James, R.J., and Rashid, J.Y.R. (2005). Severe Impact Dynamics of Reinforced Concrete Structures. Sixth European Conference on Structural Dynamics, EURODYN 2005.

[24] Forasassi, G., and Lofrano, R. (2010). Preliminary analysis of an aircraft impact. A Report of RICERCA DI SISTEMA ELETTRICO.

[25] Iliev, V., Georgiev, K., Serbezov, V. (2011). Assessment of impact load curve of Boeing 747-400, MTM Virtual Journal, 1, pp.22-25.

[26] Ouda, A.S. (2014). Development of High-Performance Heavy Density Concrete Using Different Aggregates for Gamma-Ray Shielding, HBRC Journal, https://doi.org/10.1016/j.hbrcj.2014.06.010.

Citation: Mostafa Hassan, Mohamed Ihab Sherif ELmasry and Nabil Hassan Elashkar, Structural Health Monitoring for External RC Nuclear Containment Using Various Setup of Inner Electrical Resistivity Measurements, International Journal of Civil Engineering and Technology (IJCIET), 15(1), 2024, pp. 47-65

Abstract Link: https://iaeme.com/Home/article_id/IJCIET_15_01_005
Article Link:
https://iaeme.com/MasterAdmin/Journal_uploads/IJCIET/VOLUME_15_ISSUE_1/IJCIET_15_01_005.pdf

✉ editor@iaeme.com